

**Electron states in a double quantum dot with broken axial symmetry**Krzysztof Gawarecki,<sup>1,\*</sup> Paweł Machnikowski,<sup>1</sup> and Tilmann Kuhn<sup>2</sup><sup>1</sup>*Institute of Physics, Wrocław University of Technology, 50-370 Wrocław, Poland*<sup>2</sup>*Institut für Festkörperteorie, Universität Münster, 48149 Münster, Germany*

(Received 20 February 2014; revised manuscript received 29 July 2014; published 28 August 2014)

We study theoretically the electron states in a system of two vertically stacked quantum dots. We investigate the influence of the geometrical symmetry breaking (caused by the displacement as well as the ellipticity of the dots) on the electron states. Our modeling is based on the eight-band  $\mathbf{k} \cdot \mathbf{p}$  method. We study the coupling of the  $s$  state from one dot with the  $p$  and  $d$  states from the other induced by the absence of axial symmetry. Our findings indicate that this coupling can produce a strong energy splitting at resonance (on the order of several meV) in the case of closely spaced quantum dots. Furthermore, we show that in the presence of a piezoelectric field, the direction of the displacement plays an important role in the character of the coupling.

DOI: [10.1103/PhysRevB.90.085437](https://doi.org/10.1103/PhysRevB.90.085437)

PACS number(s): 73.21.La, 73.63.Kv, 63.20.kd

**I. INTRODUCTION**

Systems composed of vertically stacked self-assembled double quantum dots (DQDs) show many interesting properties, qualitatively different from what might be observed in single-QD samples [1]. Their rich spectrum of excitonic states includes spatially direct and indirect excitons [2], that is, electron-hole configurations with the two particles in the same or in different QDs, respectively. A common way of investigating the DQD structures is to place them in a photodiode structure, which allows one not only to measure the system absorption via the induced photocurrent, but also to apply an axial electric field [3–5], which results in an intricate pattern of resonances between these two classes of states as a function of the field [3,5–8]. Apart from the external field, the nature of the carrier states and the emission spectrum of a DQD are strongly affected by band mixing [9–11] and spin-orbit coupling [8].

These unique properties of pairs of coupled QDs, combined with their relatively simple manufacturing as a result of their spontaneous formation in a Stransky-Krastanov process, have motivated many theoretical and laboratory-scale experimental proposals for their practical applications. Entanglement between the carriers in DQDs appears naturally [12] and can be optically created using robust optical control schemes [13]. Early proposals for qubit encoding in DQDs [14] have been extended to experimentally demonstrated conditional control [4] as well as decoherence protected qubits and implementations of quantum algorithms [15]. Collective emission from such structures [16] has interesting angular characteristics that allow them to be used as quantum nano-antennas [17]. Raman couplings between singlet and triplet states in DQDs result in optical gain and can be exploited to build a single emitter laser [18].

Due to their rich structure of optical transitions, DQD structures are favorable for spin control and readout [19], hence potential applications of DQD systems are sought also in the direction of spintronics and spin-based quantum computation. DQDs have been proposed to be used for spin-based quantum bits [20,21]. Spin entanglement in these

structures can be created optically [22]. Singlet-triplet qubits have been implemented on two-electron configurations in such systems [23]. Single spin preparation is possible in DQDs by fast dissociation of optically created excitons [24].

Because in stacked DQD systems the dots are placed rather close to each other, their properties are significantly affected by tunnel coupling [2,12,25–31] or by exchange coupling [23]. In both cases, precise knowledge of the electronic wave functions, including the effects of system morphology, the role of symmetry, and the possible impact of band mixing and spin-orbit couplings, is essential for correct modeling of the system properties and the functionality of possible nanodevices. While controlled charging of nanostructures with single-electron precision is experimentally achievable [32], single-electron states in DQDs are not commonly addressed in optical experiments. However, tunnel resonances between direct and indirect exciton states [5] essentially reveal single-particle properties of the tunneling particle, with the other carrier playing the role of a passive spectator (apart from shifting the energies due to Coulomb interactions).

Carrier spectra of quantum dots have been widely described in the literature using the  $\mathbf{k} \cdot \mathbf{p}$  model [26,27,33–36] as well as tight-binding and pseudopotential methods [6,37–43]. However, DQDs composed of lens-shaped QDs are often modeled assuming the axial symmetry of the system. In that approximation, the axial projection of the envelope angular momentum is conserved and there is no coupling between states with different angular momenta. On the other hand, from an experimental point of view, samples usually do not have axial symmetry [44]. Dots from different layers can be shifted with respect to each other and can be elliptical. Furthermore, axial symmetry can be broken due to composition fluctuations inside the dots. This opens the possibility of an additional coupling, which would be prohibited in an ideal (symmetric) case. Indeed, some experiments exhibit features, which suggest such a behavior [5]. In Ref. [8], the symmetry breaking in a DQD excitonic system was studied. However, those calculations were performed in the effective-mass approximation, and the deviations from axial symmetry (due to a displacement and ellipticity) have only been introduced by a small perturbative parameter. In Ref. [45], the symmetry-breaking effects on the hole anticrossing in a DQD were analyzed. Those calculations

\*Krzysztof.Gawarecki@pwr.edu.pl

were based on a four-band  $\mathbf{k} \cdot \mathbf{p}$  model including strain and a piezoelectric field. Moreover, in Ref. [46], (110)-tilted quantum dot stacks are under consideration.

In this work, we study systematically the influence of the geometrical axial symmetry breaking of arbitrary magnitude on the electron states in the structure composed of two vertically stacked QDs formed in the Stransky–Krastanov self-assembly process. We consider  $\text{In}_{0.8}\text{Ga}_{0.2}\text{As}$  dots embedded in a GaAs matrix. We calculate the strain distribution in the system using the continuous elasticity approach [47]. The piezoelectric field is included up to second order in the strain tensor [38,48], which leads to a dependence of the predicted spectral features on the direction of the system deformation with respect to the crystallographic axes. We find the electron states within the eight-band  $\mathbf{k} \cdot \mathbf{p}$  model. We show that axial symmetry breaking in a DQD structure leads to a qualitative reconstruction of the energy spectrum, in particular in the vicinity of level crossings. This effect turns out to depend crucially on the system geometry with respect to the crystallographic axes.

The paper is organized as follows. In Sec. II, we define the model. In Sec. III, we discuss the results of the obtained electron states. Finally, concluding remarks and a discussion are contained in Sec. IV.

## II. MODEL

The system under consideration contains two vertically stacked  $\text{In}_{0.8}\text{Ga}_{0.2}\text{As}$  QDs, where we assume homogeneous alloying. Both dots are placed on wetting layers (with an assumed width of 0.6 nm). Because of a lattice mismatch between InAs and GaAs, strain appears in the system. To find the strain distribution, we performed a minimization of the elastic energy of the system [47] using the continuous elasticity approach. As a result, we obtained the displacement field and the strain tensor  $\epsilon$ .

Due to a nonzero shear strain in the system, a piezoelectric (PZ) field appears and affects the carrier states [38]. To calculate the potential generated by the piezoelectricity ( $V_{\text{PZ}}$ ), we calculated the polarization of the system up to second order in the strain tensor. A detailed description of the piezoelectric field calculation is given in Appendix A.

The local band structure is derived from the eight-band  $\mathbf{k} \cdot \mathbf{p}$  Hamiltonian with the strain-induced terms. Because of its numerical advantages [49], we use the LS basis  $\{|S\uparrow\rangle, |X\uparrow\rangle, |Y\uparrow\rangle, |Z\uparrow\rangle, |S\downarrow\rangle, |X\downarrow\rangle, |Y\downarrow\rangle, |Z\downarrow\rangle\}$ , where  $S, X, Y, Z$  denote electron orbitals and  $\uparrow$  and  $\downarrow$  represent spin projection. In the matrix representation, the Hamiltonian takes the form [50,51]

$$H = \begin{pmatrix} H(\mathbf{k}) & \Gamma \\ -\Gamma^* & H(\mathbf{k}) \end{pmatrix},$$

where

$$\Gamma = \frac{\Delta}{3} \begin{pmatrix} 0 & 0 & 0 & 0 \\ 0 & 0 & 0 & 1 \\ 0 & 0 & 0 & -i \\ 0 & -1 & i & 0 \end{pmatrix}$$

and  $H(\mathbf{k}) = H_1 + H_2$ . Here

$$H_1 = \begin{pmatrix} E_s & iPk_x & iPk_y & iPk_z \\ -iPk_x & E_x & N'k_xk_y - i\frac{\Delta}{3} & N'k_xk_z \\ -iPk_y & N'k_xk_y + i\frac{\Delta}{3} & E_y & N'k_yk_z \\ -iPk_z & N'k_xk_z & N'k_yk_z & E_z \end{pmatrix}$$

and

$$H_2 = \begin{pmatrix} 0 & -iP\epsilon_{xj}k_j & -iP\epsilon_{yj}k_j & -iP\epsilon_{zj}k_j \\ iP\epsilon_{xj}k_j & 0 & n\epsilon_{xy} & n\epsilon_{xz} \\ iP\epsilon_{yj}k_j & n\epsilon_{xy} & 0 & n\epsilon_{yz} \\ iP\epsilon_{zj}k_j & n\epsilon_{xz} & n\epsilon_{yz} & 0 \end{pmatrix}.$$

The diagonal part of  $H_1$  contains

$$\begin{aligned} E_s &= A'(k_x^2 + k_y^2 + k_z^2) + E_c + a_c(\epsilon_{xx} + \epsilon_{yy} + \epsilon_{zz}), \\ E_x &= L'k_x^2 + M'(k_y^2 + k_z^2) + E'_v + l\epsilon_{xx} + m(\epsilon_{yy} + \epsilon_{zz}), \\ E_y &= L'k_y^2 + M'(k_x^2 + k_z^2) + E'_v + l\epsilon_{yy} + m(\epsilon_{xx} + \epsilon_{zz}), \\ E_z &= L'k_z^2 + M'(k_x^2 + k_y^2) + E'_v + l\epsilon_{zz} + m(\epsilon_{yy} + \epsilon_{xx}), \end{aligned}$$

with

$$\begin{aligned} E_c &= E_v + E_g + V_{\text{PZ}} + e\epsilon z, \\ E'_v &= E_v - \Delta/3 + V_{\text{PZ}} + e\epsilon z, \\ A' &= \frac{\hbar^2}{2m_0} \left( \frac{1}{m_e^*} - \frac{E_p(E_g + 2\Delta/3)}{E_g(E_g + \Delta)} \right), \\ E_p &= \frac{2m_0P^2}{\hbar^2}, \\ L' &= \frac{P^2}{E_g} - \frac{\hbar^2}{2m_0}(\gamma_1 + 4\gamma_2), \\ M' &= -\frac{\hbar^2}{2m_0}(\gamma_1 - 2\gamma_2), \\ N' &= \frac{P^2}{E_g} - \frac{3\hbar^2}{m_0}\gamma_3, \end{aligned}$$

where  $k_j = -i\partial/\partial x_j$ ,  $E_v$  denotes the unstrained average valence-band edge,  $\Delta$  is the spin-orbit split-off element,  $E_g$  is the energy gap,  $P$  is a parameter proportional to the interband momentum matrix element,  $m_0$  is the free electron mass,  $m_e^*$  is the electron effective mass in a bulk material,  $\epsilon$  denotes the axial electric field, and  $\gamma_i$  are Luttinger parameters. In  $H_2$ , the Einstein summation convention is being used. The influence of the strain field on the carrier states has been accounted for using  $l = 2b_v + a_v$ ,  $m = a_v - b_v$ ,  $n = \sqrt{3}d_v$ , where  $a_c, a_v, b_v$  are the conduction- and valence-band deformation potentials, and  $d_v$  is the shear strain deformation potential. We perform Burt-Foreman ordering [52,53], which for the upper triangular matrix is  $N'k_i k_j \rightarrow k_i N_+ k_j + k_j N_- k_i$  and for the lower one  $N'k_i k_j \rightarrow k_j N_+ k_i + k_i N_- k_j$ , where  $N_- = M' - \hbar^2/2m_0$  and  $N_+ = N' - N_-$ . To avoid spurious solutions, we use the reduced value of  $E_p$  [51]. The wave functions were calculated within the envelope function approximation (EFA) [54].

Spin-orbit coupling (the Dresselhaus term) in the conduction band is neglected. The values of the material parameters are given in Table I. The resulting eigenproblem is solved using the Jacobi-Davidson method. All details of the calculations have been described in Appendix B. Finally, the in-plane

TABLE I. Material parameters used in the calculations [33,55].

	GaAs	InAs	Interpolation of In <sub>x</sub> Ga <sub>1-x</sub> As
$E_{v0}$	0.0 eV	0.173 eV	$0.173x + 0.058x(1-x)$
$E_g$	1.518 eV	0.413 eV	$0.413x + 1.518(1-x) - 0.477x(1-x)$
$E_p$	21.0 eV	18.0 eV	$18.0x + 21.0(1-x) + 1.48x(1-x)$
$m_e^*$	0.065	0.022	$0.022x + 0.065(1-x) - 0.0091x(1-x)$
$\Delta$	0.34 eV	0.38 eV	$0.38x + 0.34(1-x) - 0.15x(1-x)$
$a_c$	-7.17 eV	-5.08 eV	$-5.08x - 7.17(1-x) - 2.61x(1-x)$
$a_v$	1.16 eV	1.0 eV	linear
$b_v$	-1.824 eV	-1.8 eV	linear
$d_v$	-5.062 eV	-3.6 eV	linear
$\gamma_1$	19.7	7.1	linear
$\gamma_2$	8.4	2.02	linear
$\gamma_3$	9.3	2.91	linear
$e_{14}$	0.230 C/m <sup>2</sup>	0.115 C/m <sup>2</sup>	linear
$B_{114}$	-0.439 C/m <sup>2</sup>	-0.531 C/m <sup>2</sup>	linear
$B_{124}$	-3.765 C/m <sup>2</sup>	-4.076 C/m <sup>2</sup>	linear
$B_{156}$	-0.492 C/m <sup>2</sup>	-0.120 C/m <sup>2</sup>	linear

probability density of the  $i$ th state is calculated according to

$$\rho_i(x, y) = \sum_{m=1}^8 \int_{-\infty}^{\infty} \psi_{i,m}^*(x, y, z) \psi_{i,m}(x, y, z) dz,$$

where  $\psi_{i,m}(x, y, z)$  is the  $m$ th component (subband) of the  $i$ th eigenfunction.

### III. RESULTS

In this section, we discuss the results of our calculations performed for a single QD as well as for a DQD.

#### A. Single QDs

First, in order to provide a clear interpretation of the results for a DQD, to be presented below, we calculated the electron states in a single QD. Each column of Fig. 1 presents the in-plane probability density of the six lowest electron states (e1–e6). We consider four cases: a circular (i.e., axially symmetric) lens-shaped QD with and without the PZ field, as well as an elliptical QD with and without the PZ field. The first column corresponds to the ideal case (circular lens-shaped QD without the PZ field). At this point, our results reflect the well-known properties of a single QD [33,38]. The ground state (e1) has an  $s$ -type symmetry. Since the system has axial symmetry, the projection of the envelope angular momentum  $M$  is a good quantum number, and the ground state corresponds to  $n = 0$  and  $M = 0$ , where  $n$  denotes the excitation of the radial part of the wave function. The next two states (e2, e3) show  $p$ -type symmetry (that is,  $n = 0$  and  $M = -1, 1$ ). Subsequently, e4, e5, and e6 exhibit  $d$  character. The states e4 and e5 correspond to the degenerate states with  $n = 0$  and  $M = -2, 2$ . Due to numerical reasons (the discretization on a rectangular grid), the degeneracy is slightly lifted and two linear combinations of these states appear that are rotated with respect to each other by 45°. In the case of e6, we have clearly  $n = 1$  with  $M = 0$ .

In the presence of the piezoelectric field (second column of Fig. 1), the character of the states is different. Due to the piezoelectric field, the symmetry of the system is lowered from

$C_{\infty}$  to  $C_{2v}$  [38]. In that case,  $M$  is no longer a good quantum number. The contribution from the second-order term of the piezoelectric field has an opposite sign to the first-order term and is important [38,48]. However, in the case of an alloy, the second-order contribution is lowered due to its dependence on the hydrostatic strain, which vanishes with increasing Ga admixture [6]. Now, the direction along the lower values of the PZ field is favored. The  $p$  states are clearly combined into orbitals  $p_1 \sim \sin(\varphi - \pi/4)$  and  $p_2 \sim \cos(\varphi - \pi/4)$ , which have mutually perpendicular orientation. Furthermore, the character of the  $d$  states is significantly changed. The e4 and e6 states couple and change their symmetry. The e5 state, which is compatible with the symmetry of the PZ field, remains uncoupled. In the third and fourth columns of Fig. 1, the results for an elliptical QD (with the major to minor axis ratio of 1.1) elongated in the (110) direction are shown. In that case, even without a PZ field, the axial symmetry is broken and the states that are elongated in the direction of the major axis are lowered in energy compared to the states elongated in the direction of the minor axis. In the case of an ellipticity ratio of 1.1, and adding the PZ field, the orientation of the  $p$  states (as in the case of the circular QD with the PZ field) is restored. Furthermore, for the  $d$  states, the PZ field essentially compensates the elliptical anisotropy such that the spatial profiles of the circular QD without the PZ field are recovered.

To check the importance of the valence-band to conduction-band coupling in the  $\mathbf{k} \cdot \mathbf{p}$  Hamiltonian, we compared our results with those obtained from a single-band effective-mass calculation based on the Löwdin elimination method [56]. The difference between the relative shell energy levels in both cases is up to 31%.

#### B. Double QDs

Next, let us consider a DQD system with a geometrical axial symmetry. A schematic diagram that illustrates the energy structure in a DQD (where the dots have different sizes) is shown in Fig. 2. The electronic structure can be tuned by

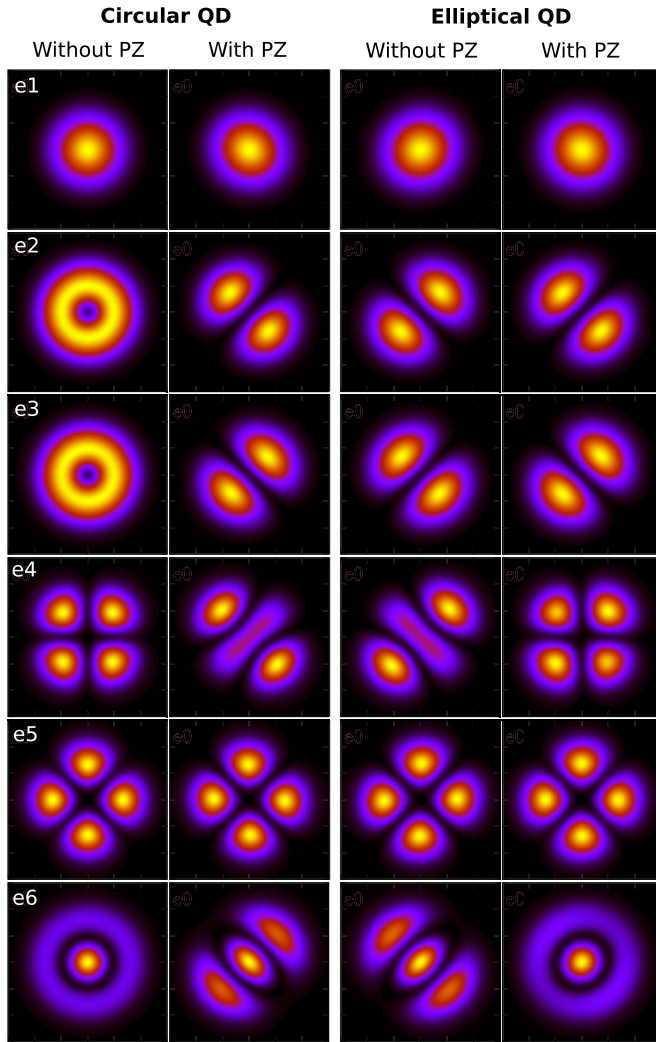


FIG. 1. (Color online) The in-plane probability density of the six lowest electron states. The first column corresponds to a circular lens-shaped QD in an ideal case (without a PZ field). The second one shows the same QD but in the presence of the PZ field. The third column presents the results for an elliptical QD without a PZ field. The last column contains results for an elliptical QD with the PZ field.

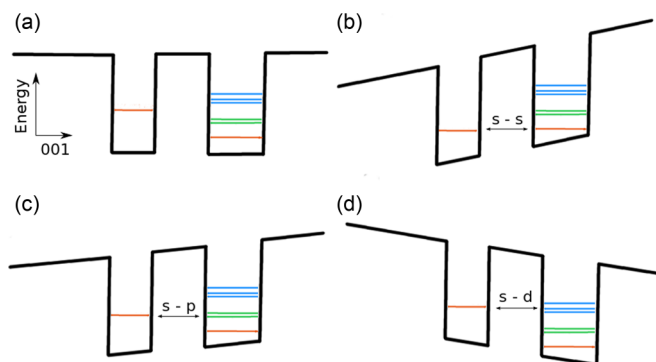


FIG. 2. (Color online) Schematic electron energy structure in the investigated DQD without (a) and with different values of an electric field (b)–(d) indicating resonances between energy levels in the two dots.

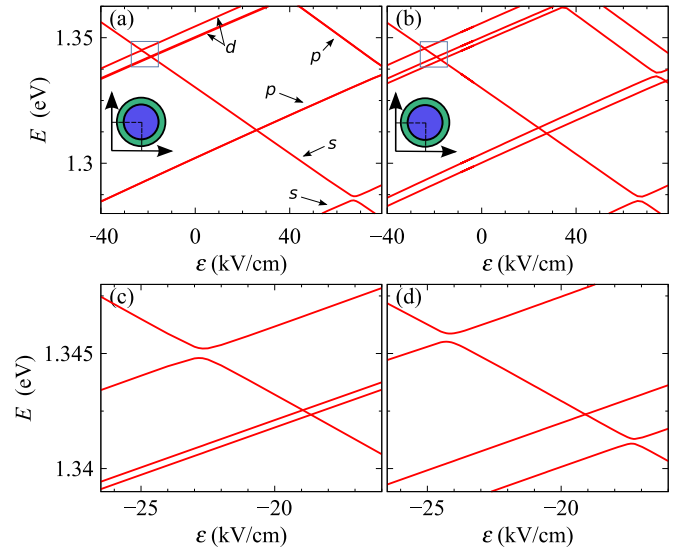


FIG. 3. (Color online) (a) Lowest electron energy branches as a function of the electric field without a PZ field. (b) The same as (a) but with the piezoelectric field included. (c) Enlarged region of (a) with  $s$ - $d$  resonances (indicated by the blue rectangle). (d) Enlarged region of (b) with  $s$ - $d$  resonances.

applying an axial electric field that modifies the slopes of the band edges. From the experimental point of view, in a DQD system, the upper dot is often bigger than the lower one [57]. Furthermore, in order to have  $s$ - $p$  and  $s$ - $d$  resonances at a reasonable value of the electric field, we assumed  $r_1 = 9$  nm,  $h_1 = 3.3$  nm and  $r_2 = 12.6$  nm,  $h_2 = 5.4$  nm, where  $r_1, h_1$  and  $r_2, h_2$  are the base radius and height of the lower and the upper dot, respectively [29].

The electron energy levels for a fixed distance  $D = 10.2$  nm between the dots (counted from the base of the lower dot to the base of the upper one) are shown in Figs. 3(a) and 3(b). The dots are placed along the same  $z$  (001) axis, and the energy branches are shown as a function of the axial electric field. Figure 3(a) presents the results without the piezoelectric field. At  $\epsilon = 67.1$  kV/cm, the electron  $s$  states in both dots have similar energy [as shown in Fig. 2(b)]. Because the symmetry of these states allows them to couple, the energies show an anticrossing. At  $\epsilon = 26$  kV/cm,  $s$  and  $p$  states become degenerate [as shown in Fig. 2(c)]. In this case, the  $p$  states are degenerate and there is no coupling between them and the  $s$ -type state from the second dot. As a consequence, there is a crossing between the energy branches.

The energy branches in the presence of the piezoelectric field are shown in Fig. 3(b). Because of the symmetry reduction due to the piezoelectric field, the electron states of type  $p$  and  $d$  are no longer degenerate. The splitting due to the PZ field is larger in the case of  $p$  states than  $d$  states, which is consistent with Ref. [6]. However, in contrast to Ref. [6], we do not observe mixing between  $s$  and  $p$  states due to the PZ field. Moreover, due to the influence of strain and the related piezoelectric field from the lower dot, the lowest state in the upper one is shifted up by about 1.5 meV. Figures 3(c) and 3(d) present an enlarged part (marked by the blue box) of Figs. 3(a) and 3(b), respectively. Figure 3(c) shows that in the absence

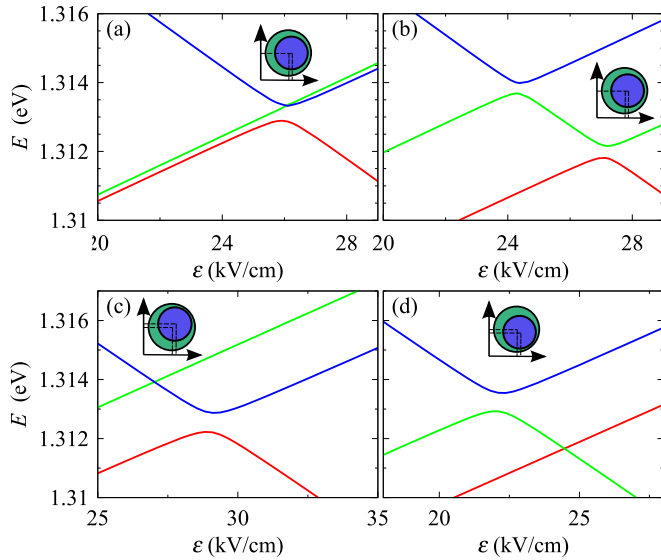


FIG. 4. (Color online) Energy branches of  $s$  and  $p$  states (a) without piezoelectric field for a shift of  $x_s = 1.8$  nm, (b) with included piezoelectric field and a shift of  $x_s = 1.8$  nm, (c) with included piezoelectric field and  $x_s = y_s = 1.8$  nm, and (d) with included piezoelectric field and  $x_s = 1.8$  nm,  $y_s = -1.8$  nm.

of a piezoelectric field, the  $s$  and the two lowest  $d$  states are decoupled and the only anticrossing in this region appears between the  $s$  state and the  $d$  state with  $M = 0$  (e6 in Fig. 1). The small splitting visible between the two lowest  $d$  states is a numerical artifact caused by the discretization. The situation changes when the piezoelectric field is included. Then, the localization of one of the uncoupled  $d$  states (e4 in Fig. 1) is partially moved to the middle of the QD. As a consequence, the symmetry changes and a coupling appear. However, the character of the second state (e5 in Fig. 1) is unchanged, thus the second crossing still remains unsplit.

To study the symmetry-breaking effects in a DQD, we displaced the lower dot in the plane perpendicular to the  $z$  axis and we investigated the  $s$ - $p$  coupling. As a result of QD size asymmetry and an appropriately chosen magnitude of the electric field, both  $p$  states are localized in the upper dot and the  $s$  state is localized in the lower one. Figure 4(a) presents the energy branches for the interesting electric field range where the lower dot is shifted in the (100) direction by  $x_s = 1.8$  nm (that is, 10% of the diameter of the lower dot) and the piezoelectric field is not taken into account. The lowest  $p$  state tends to be oriented along the direction of the displacement, and the second one is perpendicular to it. As a result of the symmetry, the  $s$  state is coupled to the first  $p$  state and uncoupled to the second one. The situation is different if the PZ field is included since this field forces alignment with respect to the (110) direction and this effect is much stronger than that resulting from the displacement [Fig. 4(b)]. Therefore, the  $p$  states in the upper dot are oriented along the (110) and (1 $\bar{1}$ 0) directions, respectively. As a consequence, both the resonances between the  $s$  and both  $p$  states are opened and show a similar splitting in both cases. However, if the QDs are displaced in the (110) direction, then even in the presence of the PZ field, only one coupling is nonzero. As can be seen in Figs. 4(c) and 4(d), a shift by  $x_s = y_s = 1.8$  nm and

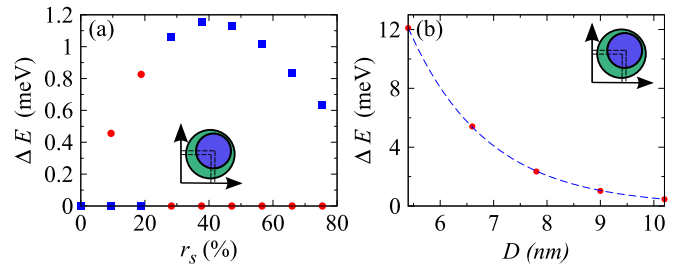


FIG. 5. (Color online) (a) The values of the energy splitting at the resonances between the  $s$  and lower  $p$  state (red circles) and higher  $p$  state (blue boxes) for  $D = 10.2$  nm as a function of the value of the relative displacement of the lower dot  $r_s$ . (b) The values of the energy splitting at the resonances between the  $s$  state and lower  $p$  state for  $x_s = y_s = 1.8$  nm, i.e.,  $r_s = 14\%$  as a function of  $D$ . The red points represents the simulation results and the blue dashed line is an exponential fitting.

$x_s = 1.8$  nm,  $y_s = -1.8$  nm opens only the first or the second  $s$ - $p$  resonance, respectively.

We investigated the dependence of the  $s$ - $p$  coupling (as reflected by the width of the resonant splitting) on the value of the shift in the (110) direction. Figure 5(a) shows the values of both resonant  $s$ - $p$  splittings as a function of the relative displacement  $r_s = \sqrt{x_s^2 + y_s^2}/2r_1$  in the presence of the PZ field. In the case of a DQD with geometrical axial symmetry ( $r_s = 0$ ), the order of the  $p$  states in the higher dot is opposite to the single QD case (e2,e3 in Fig. 1). It is caused by the influence of the PZ field from the lower dot [6]. On the other hand, the influence of the PZ field from the upper dot on the  $s$  state in the lower one plays a minor role. For a small shift in the (110) direction, the lower  $p$  state is coupled and the second one remains decoupled. However, for shifts larger than about 25%, the ordering of the  $p$  states is reversed and the situation from a single QD is restored. In that case, the lower  $p$  state is uncoupled and the higher one is coupled. The dependence of the splitting on the value of the shift is determined by two processes: on the one hand, increasing the displacement (in some range) enhances the  $s$ - $p$  coupling, but on the other hand, the overlap between the wave functions decreases with the shift. As a result, the splitting has a maximum at a relative displacement near 40% of the lower dot size.

We investigated also the dependence of the  $s$ - $p$  splitting on the distance  $D$  between the dots. Figure 5(b) presents this splitting in the case of the constant shift value  $x_s = y_s = 1.8$  nm as a function of the distance  $D$ . As we can see, the dependence is nearly exponential. The splitting width ( $\Delta E$ ) is very well fitted by the formula  $\ln(\Delta E/E_0) = -\kappa D$ , with parameters  $\kappa = 0.678$  nm $^{-1}$  and  $E_0 = 0.472$  eV (for the displacement  $x_s = y_s = 1.8$  nm). The  $s$ - $p$  splitting calculated in the eight-band  $\mathbf{k} \cdot \mathbf{p}$  model is in good agreement with that obtained from the single-band approach (the value from the single-band model is about 5% lower).

We also investigated the influence of symmetry breaking on the  $s$ - $d$  coupling. As presented in Fig. 3(d), the coupling between the  $s$  and the two  $d$  states can appear even if the geometrical symmetry is conserved and is a consequence of the PZ field. Here, we investigate the effects of symmetry breaking in two cases: the shift along the (100) direction and

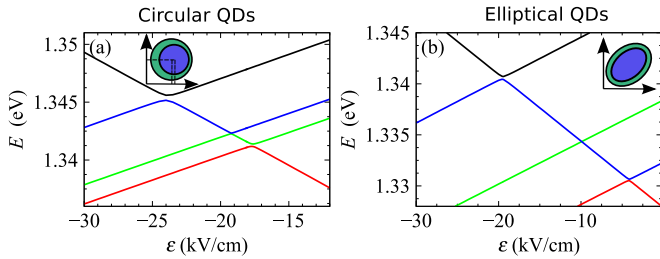


FIG. 6. (Color online) (a) Energy branches as a function of the electric field in the region of the  $s$ - $d$  resonances at  $x_s = 1.8$  nm with  $y_s = 0$ . (b) Energy branches as a function of electric field in the region of the  $s$ - $d$  resonances in the case of elliptical dots.

the situation where both dots are elliptical. In the case of the shift [Fig. 6(a)] by  $x_s = 1.8$  nm with  $y_s = 0$ , a mixing between the  $s$  state and the second  $d$  state becomes possible. However, this coupling is weak and only a small splitting in the resonance appears (of the order of  $66 \mu\text{eV}$ ). Also for the first and third  $d$  state, the effect is relatively small and we obtain splitting values comparable to those resulting only from the PZ field. The reason is that a shift in the (100) direction conserves the mirror symmetry in the (010) direction, which is also important from the point of view of coupling.

In the next step, we consider both dots to have an elliptical shape with the major to minor axis ratio of 1.1 where the elongation is in the (110) direction. Due to symmetry reasons, ellipticity does not lead to  $s$ - $p$  mixing. Although this mixing appears if the higher-order SO coupling is included, its value is small (about  $100 \mu\text{eV}$  at  $D = 10$  nm) [8]. The results for elliptical dots in the region of the  $s$ - $d$  resonances are shown in Fig. 6(b). From a qualitative point of view, an elongation in the (110) direction does not change the situation from Fig. 3(d), that is,  $s$  is coupled only to the first and third  $d$  state. However, this leads in particular to a reduction of the width of the resonance between the  $s$  and the lowest  $d$  state.

#### IV. CONCLUSIONS

In summary, we have studied the effects of coupling between the electron states from different subshells ( $s, p, d$ ) localized in different dots in a DQD structure, taking into account the orientation of the system geometry with respect to the crystallographic axes. We have shown that breaking of the geometrical axial symmetry by a relative off-axial shift of the dots can lead to strong  $s$ - $p$  mixing. We have found out that in the presence of the piezoelectric field, the direction of the shift plays an important role in the electronic structure. We have also shown that  $s$ - $p$  resonances are much more sensitive to the geometrical symmetry breaking than  $s$ - $d$  resonances. We have studied the influence of dot ellipticity on the  $s$ - $d$  resonances, and we have shown that those effects give only a quantitative correction to the effect resulting from the piezoelectric field.

#### ACKNOWLEDGMENTS

We are grateful to Janusz Andrzejewski, Jonas Daniels, and Juan Climente for inspiring discussion, as well as to Thomas Kendziorczyk for many useful numerical clues. This work was partly supported by the Foundation for Polish Science under

the TEAM programme, cofinanced by the European Regional Development Fund. K.G. acknowledges support from the German Academic Exchange Service (DAAD).

#### APPENDIX A: PIEZOELECTRIC FIELD

To calculate the potential generated by the piezoelectricity, we found the polarization  $\mathbf{P} = \mathbf{P}_1 + \mathbf{P}_2$  up to second order in the strain tensor. In the case of zinc-blende structure growth in the (001) direction, it takes the form [48,58,59]

$$\mathbf{P}_1 = e_{14} \begin{pmatrix} \epsilon_{yz} \\ \epsilon_{xz} \\ \epsilon_{xy} \end{pmatrix},$$

$$\mathbf{P}_2 = 2B_{114} \begin{pmatrix} \epsilon_{xx}\epsilon_{yz} \\ \epsilon_{yy}\epsilon_{xz} \\ \epsilon_{zz}\epsilon_{xy} \end{pmatrix} + 2B_{124} \begin{pmatrix} (\epsilon_{yy} + \epsilon_{zz})\epsilon_{yz} \\ (\epsilon_{xx} + \epsilon_{zz})\epsilon_{xz} \\ (\epsilon_{xx} + \epsilon_{yy})\epsilon_{xy} \end{pmatrix} + 4B_{156} \begin{pmatrix} \epsilon_{xz}\epsilon_{xy} \\ \epsilon_{yz}\epsilon_{xy} \\ \epsilon_{yz}\epsilon_{xz} \end{pmatrix},$$

where  $e_{14}$  and  $B_{114}, B_{124}, B_{156}$  are linear and quadratic polarization parameters, respectively. Then, the piezoelectricity-induced charge is calculated from  $\rho_{\text{piezo}} = -\nabla \cdot \mathbf{P}$ . Finally, the piezoelectric potential  $V_p$  is found from the solution of the Poisson-like equation,

$$\rho_{\text{piezo}} = \epsilon_0 \nabla [\epsilon_S(\mathbf{r}) \nabla V_p],$$

where  $\epsilon_S(\mathbf{r})$  is the position-dependent static dielectric constant.

#### APPENDIX B: CALCULATION DETAILS

We have performed the calculation of the strain tensor as well as the electron states. We have used a nonuniform grid ( $160 \times 160 \times 160$ ) with mesh size nearly half of the InAs lattice constant (0.3 nm) inside the QDs and with size linearly increasing outside the QDs. To calculate the displacement field and the piezoelectric field, we have solved numerically a linear set of equations using the GMRES method combined with the ILU preconditioner with the LIS library [60]. The electron states are found using the Jacobi-Davidson method (which allows us to obtain the eigenvalues from the middle of the energy spectrum due to the spectral transformation) in the SLEPC library [61] combined with the PETSC library [62]. The wave functions were calculated within the EFA approximation on a grid. Second-order derivatives have been discretized according to the finite-difference scheme [63],

$$\frac{\partial}{\partial x_k} \left( A \frac{\partial}{\partial x_k} B \right) = \frac{B_{i+1} - B_i}{h_i(h_i + h_{i-1})} (A_{i+1} + A_i) + \frac{B_{i-1} - B_i}{h_i(h_i + h_{i-1})} (A_{i-1} + A_i),$$

where  $h_i$  is a position-dependent mesh size. Such discretization leads to an asymmetric matrix in the eigenvalue problem. To restore symmetrization, we applied an appropriate transformation as described in Ref. [63].

- [1] J. Wu and Z. M. Wang, *Quantum Dot Molecules* (Springer, New York, 2014).
- [2] B. Szafran, S. Bednarek, and J. Adamowski, *Phys. Rev. B* **64**, 125301 (2001).
- [3] H. J. Krenner, M. Sabathil, E. C. Clark, A. Kress, D. Schuh, M. Bichler, G. Abstreiter, and J. J. Finley, *Phys. Rev. Lett.* **94**, 057402 (2005).
- [4] L. Robledo, J. Elzerman, G. Jundt, M. Atatüre, A. Högele, S. Fält, and A. Imamoglu, *Science* **320**, 772 (2008).
- [5] K. Müller, A. Bechtold, C. Ruppert, M. Zecherle, G. Reithmaier, M. Bichler, H. J. Krenner, G. Abstreiter, A. W. Holleitner, J. M. Villas-Boas, M. Betz, and J. J. Finley, *Phys. Rev. Lett.* **108**, 197402 (2012).
- [6] M. Usman, Y.-H. M. Tan, H. Ryu, S. S. Ahmed, H. J. Krenner, T. B. Boykin, and G. Klimeck, *Nanotechnology* **22**, 315709 (2011).
- [7] K. Müller, G. Reithmaier, E. C. Clark, V. Jovanov, M. Bichler, H. J. Krenner, M. Betz, G. Abstreiter, and J. J. Finley, *Phys. Rev. B* **84**, 081302 (2011).
- [8] J. M. Daniels, P. Machnikowski, and T. Kuhn, *Phys. Rev. B* **88**, 205307 (2013).
- [9] W. Jaskólski, M. Zieliński, G. W. Bryant, and J. Aizpurua, *Phys. Rev. B* **74**, 195339 (2006).
- [10] M. F. Doty, J. I. Climente, M. Korkusinski, M. Scheibner, A. S. Bracker, P. Hawrylak, and D. Gammon, *Phys. Rev. Lett.* **102**, 047401 (2009).
- [11] W. J. Pasek and B. Szafran, *Phys. Rev. B* **85**, 085301 (2012).
- [12] M. Bayer, P. Hawrylak, K. Hinzer, S. Fafard, M. Korkusinski, Z. R. Wasilewski, O. Stern, and A. Forchel, *Science* **291**, 451 (2001).
- [13] C. Creatore, R. T. Brierley, R. T. Phillips, P. B. Littlewood, and P. R. Eastham, *Phys. Rev. B* **86**, 155442 (2012).
- [14] E. Biolatti, R. C. Iotti, P. Zanardi, and F. Rossi, *Phys. Rev. Lett.* **85**, 5647 (2000).
- [15] M. M. Santos, F. O. Prado, H. S. Borges, A. M. Alcalde, J. M. Villas-Bôas, and E. I. Duzzioni, *Phys. Rev. A* **85**, 032323 (2012).
- [16] A. Sitek and P. Machnikowski, *Phys. Rev. B* **75**, 035328 (2007).
- [17] S. Mokhlespour, J. E. M. Haverkort, G. Slepyan, S. Maksimenko, and A. Hoffmann, *Phys. Rev. B* **86**, 245322 (2012).
- [18] J. M. Elzerman, K. M. Weiss, J. Miguel-Sanchez, and A. Imamoglu, *Phys. Rev. Lett.* **107**, 017401 (2011).
- [19] A. N. Vamivakas, C.-Y. Lu, C. Matthiesen, Y. Zhao, S. Fält, A. Badolato, and M. Atatüre, *Nature (London)* **467**, 297 (2010).
- [20] M. F. Doty, J. I. Climente, A. Greilich, M. Yakes, A. S. Bracker, and D. Gammon, *Phys. Rev. B* **81**, 035308 (2010).
- [21] S. E. Economou, J. I. Climente, A. Badolato, A. S. Bracker, D. Gammon, and M. F. Doty, *Phys. Rev. B* **86**, 085319 (2012).
- [22] D. Kim, S. G. Carter, A. Greilich, A. S. Bracker, and D. Gammon, *Nat. Phys.* **7**, 223 (2010).
- [23] K. M. Weiss, J. M. Elzerman, Y. L. Delley, J. Miguel-Sanchez, and A. Imamoglu, *Phys. Rev. Lett.* **109**, 107401 (2012).
- [24] K. Müller, A. Bechtold, C. Ruppert, C. Hautmann, J. S. Wildmann, T. Kaldewey, M. Bichler, H. J. Krenner, G. Abstreiter, M. Betz, and J. J. Finley, *Phys. Rev. B* **85**, 241306 (2012).
- [25] G. W. Bryant, *Phys. Rev. B* **47**, 1683 (1993).
- [26] M. Korkusiński and P. Hawrylak, *Phys. Rev. B* **63**, 195311 (2001).
- [27] A. Schliwa, O. Stier, R. Heitz, M. Grundmann, and D. Bimberg, *Phys. Status Solidi B* **224**, 405 (2001).
- [28] G. Bester, J. Shumway, and A. Zunger, *Phys. Rev. Lett.* **93**, 047401 (2004).
- [29] K. Gawarecki, M. Pochwała, A. Grodecka-Grad, and P. Machnikowski, *Phys. Rev. B* **81**, 245312 (2010).
- [30] K. Gawarecki and P. Machnikowski, *Acta Phys. Pol. A* **119**, 637 (2011).
- [31] K. Gawarecki and P. Machnikowski, *Phys. Rev. B* **85**, 041305 (2012).
- [32] M. Atatüre, J. Dreiser, A. Badolato, A. Högele, K. Karrai, and A. Imamoglu, *Science* **312**, 551 (2006).
- [33] A. Schliwa, M. Winkelkemper, and D. Bimberg, *Phys. Rev. B* **76**, 205324 (2007).
- [34] O. Stier, M. Grundmann, and D. Bimberg, *Phys. Rev. B* **59**, 5688 (1999).
- [35] J. Andrzejewski, G. Şek, E. O'Reilly, A. Fiore, and J. Misiewicz, *J. Appl. Phys.* **107**, 073509 (2010).
- [36] L. Voon and M. Willatzen, *The K P Method: Electronic Properties of Semiconductors* (Springer-Verlag, Berlin, 2009).
- [37] G. Bester and A. Zunger, *Phys. Rev. B* **71**, 045318 (2005).
- [38] G. Bester, A. Zunger, X. Wu, and D. Vanderbilt, *Phys. Rev. B* **74**, 081305 (2006).
- [39] A. J. Williamson, L. W. Wang, and A. Zunger, *Phys. Rev. B* **62**, 12963 (2000).
- [40] S. Sundaresan, S. Islam, and S. Ahmed, in *Nanotechnology Materials and Devices Conference (NMDC)* (IEEE, Monterey, CA, 2010), pp. 30–35.
- [41] M. Zieliński, *Phys. Rev. B* **86**, 115424 (2012).
- [42] M. Zieliński, *J. Phys.: Condens. Matter* **25**, 465301 (2013).
- [43] M. Usman, *Phys. Rev. B* **86**, 155444 (2012).
- [44] Y. Q. Wang, Z. Wang, J. Shen, and A. Brown, *Solid State Commun.* **122**, 553 (2002).
- [45] F. Rajadell, J. I. Climente, and J. Planelles, *Appl. Phys. Lett.* **103**, 132105 (2013).
- [46] M. Usman, *Phys. Rev. B* **89**, 081302 (2014).
- [47] C. Pryor, J. Kim, L. W. Wang, A. J. Williamson, and A. Zunger, *J. Appl. Phys.* **83**, 2548 (1998).
- [48] G. Bester, X. Wu, D. Vanderbilt, and A. Zunger, *Phys. Rev. Lett.* **96**, 187602 (2006).
- [49] J. Andrzejewski, *J. Comput. Phys.* **249**, 22 (2013).
- [50] A. Schliwa, Ph.D. thesis, The Technical University of Berlin, 2007.
- [51] G. Yong-Xian, Y. Tao, J. Hai-Ming, X. Peng-Fei, and W. Zhan-Guo, *Chin. Phys. B* **19**, 088102 (2010).
- [52] M. G. Burt, *J. Phys.: Condens. Matter* **4**, 6651 (1992).
- [53] B. A. Foreman, *Phys. Rev. B* **56**, R12748 (1997).
- [54] R. Winkler, *Spin-Orbit Coupling Effects in Two-Dimensional Electron and Hole Systems*, Springer Tracts in Modern Physics Vol. 191 (Springer, Berlin, 2003).
- [55] I. Vurgaftman, J. R. Meyer, and L. R. Ram-Mohan, *J. Appl. Phys.* **89**, 5815 (2001).
- [56] P. O. Löwdin, *J. Chem. Phys.* **19**, 1396 (1951).
- [57] H. J. Krenner, S. Stuffer, M. Sabathil, E. C. Clark, P. Ester, M. Bichler, G. Abstreiter, J. J. Finley, and A. Zrenner, *New J. Phys.* **7**, 184 (2005).
- [58] S. Schulz, M. A. Caro, E. P. O'Reilly, and O. Marquardt, *Phys. Rev. B* **84**, 125312 (2011).
- [59] S. Schulz, M. A. Caro, E. P. O'Reilly, and O. Marquardt, *Phys. Status Solidi B* **249**, 521 (2012).

- [60] A. Nishida, *Computational Science and Its Applications—ICCSA 2010*, Lecture Notes in Computer Science Vol. 6017 (Springer, Berlin, 2010), pp. 448–462.
- [61] V. Hernandez, J. E. Roman, and V. Vidal, *ACM Trans. Math. Software* **31**, 351 (2005).
- [62] S. Balay, S. Abhyankar, M. F. Adams, J. Brown, P. Brune, K. Buschelman, V. Eijkhout, W. D. Gropp, D. Kaushik, M. G. Knepley, L. C. McInnes, K. Rupp, B. F. Smith, and H. Zhang, PETSc (2014), <http://www.mcs.anl.gov/petsc>
- [63] I.-H. Tan, G. L. Snider, L. D. Chang, and E. L. Hu, *J. Appl. Phys.* **68**, 4071 (1990).